Eur. Phys. J. D **19**, 293–305 (2002)
DOI: 10.1140/epjd/e20020082

THE EUROPEAN PHYSICAL JOURNAL D
EDP Sciences

Quantum chemical construction of a reduced reaction Hamiltonian and T_1-relaxation and pure T_2-dephasing rates for the proton transfer in 3-chlorotropolone

R. Xu[1,a], Y.J. Yan[1], and O. Kühn[2]

[1] Open Laboratory of Bond-Selective Chemistry, University of Science and Technology of China, Hefei, China and Department of Chemistry, Hong Kong University of Science and Technology, Kowloon, Hong Kong SAR, P.R. China
[2] Institut für Chemie, Physikalische und Theoretische Chemie, Freie Universität Berlin, Takustrasse 3, 14195 Berlin, Germany

Received 19 November 2001 and Received in final form 19 February 2002

Abstract. Separating multidimensional problems into that of a relevant system which is coupled to a bath of harmonic oscillators is a common concept in condensed phase theory. Focusing on the specific problem of intramolecular proton transfer in an isolated tropolone derivative, we consider the reactive proton moving in the plane of the molecule as the system and the remaining substrate normal modes as the bath. An all-Cartesian system-plus-substrate Hamiltonian is constructed employing density functional theory. It is then used to determine the temperature-dependent effective reduced reaction Hamiltonian and the state-to-state dissipation rates induced *via* the system-substrate coupling up to the bi-quadratic order. The important substrate modes for the T_1-relaxation and the pure T_2-dephasing rates, which are either intra- or inter-well in nature, are identified numerically and analyzed physically with molecular details.

PACS. 31.70.Hq Time-dependent phenomena: excitation and relaxation processes, and reaction rates – 82.30.Qt Isomerization and rearrangement – 31.15.Ar Ab initio calculations

1 Introduction

A molecular Hamiltonian is the basic ingredient for any dynamics simulation. Within the Born-Oppenheimer approximation the nuclear motions take place on an adiabatic potential energy surface (PES), $U(\mathbf{R})$, which in principle should be evaluated on an *ab initio* level of quantum chemistry. However, since $U(\mathbf{R})$ is a function of the $3N-6$ molecular degrees of freedom (DOF), its complete *ab initio* determination becomes practically impossible if there are more than 3 or 4 atoms involved.

The development of approximate approaches makes use of the fact that reaction dynamics quite often involves large-amplitude motions of only a few atoms or modes which are referred to as the *reaction coordinates*. The majority of atoms or modes are merely spectators comprising the *substrate* and performing only small amplitude vibrations around their equilibrium positions during the reaction. Commonly, a reaction path is considered which coincides with the steepest descent or minimum energy path from the transition state. This path contains important information on the chemical reaction such as the energetics of different conformations and the way they are connected [1,2]. However, in view of dynamics, restricting a reaction to only a one-dimensional reaction coordinate without incorporating its correlation with the other $3N-7$ DOF of the substrate, may not be a valid approximation.

In a classic paper, Miller *et al.* [3] derived a reaction path Hamiltonian which includes the effect of the substrate on the reaction dynamics. Specifically, they defined local normal modes orthogonal to the reaction path which implies the validity of a second order Taylor expansion. An extension in terms of a reaction surface defined by several internal coordinates was also given [4,5]. Here, the effective Hamiltonian for the reaction surface takes the traditional Wilson form [6]. The problem of a formulation in terms of internal or minimum energy path coordinates is that the kinetic energy operator contains the couplings among the various DOF due to Coriolis-type interactions and the curvature change along the reaction path. This type of kinetic energy operator is difficult to calculate numerically especially in intramolecular proton transfer (PT) systems where the reaction paths are sharply curved.

An alternative has been shown to be a *Cartesian* reaction Hamiltonian (CRH) description [7]. Here, the Cartesian coordinates of reactive atoms/modes are chosen as the system, while those of the substrate are transferred

[a] In partial fulfillment of the requirement for PhD degree at USTC. e-mail: rxxu@mail.ustc.edu.cn

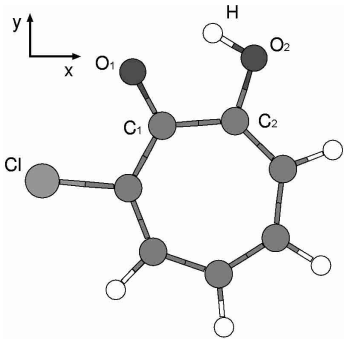

Fig. 1. Most stable isomer (E1) of 3CTR as calculated using the DFT/B3LYP method with the Gaussian basis set 6-31+G(d, p). The coordinate system for defining the reaction surface for PT is also shown (see text).

into normal modes with reference to a specific molecular configuration. The Cartesian form of the Hamiltonian has the advantage that the kinetic energy operator is diagonal and all couplings are in the potential. Nevertheless, the CRH has only recently been implemented numerically at an *ab initio* level for polyatomic molecular systems [8–10]. Note that this approach is closely related to the Cartesian form of the modified Shepard interpolation method which has been used to calculate the tunnel splitting in malonaldehyde recently [11].

For multidimensional quantum dynamics simulation, the (multiconfiguration) time-dependent self-consistent field method [12–16] for solving the Schrödinger equation has shown to be practical [17–20]. On the other hand, the CRH resembles the generic system-bath Hamiltonian that is widely used in the theory of condensed phase dynamics [21–24]. This makes it possible to simulate the dynamics *via* reduced density matrix theory in terms of quantum dissipation. This approach was recently exploited by Kühn and coworkers [25–27]. In their work, the reduced reaction PES was constructed for the PT in thiocetylacetone as a parameterized function based on some *ab initio* evaluated sampling points. The effect of substrate DOF was taken into account in terms of the interaction spectral density which was assumed to be of the empirical ohmic form [23] with a cut-off frequency typical for the low frequency molecular vibrations [25–27].

In the present work, a reduced description will be adopted as well but based on an fully quantum chemically constructed CRH in the ground electronic (S_0) state for the correlated system-plus-substrate PT dynamics in 3-chlorotropolone (3CTR), see Figure 1. Tropolone and its derivatives have attracted considerable attention [28–34]. There is experimental evidence that the PT in these systems is not just a simple motion of the proton. Certain collective motions of heavy atoms of the molecular frame play an important role as well, *e.g.* for the tunnelling dynamics. To identify these collective substrate motions at a molecular level and to correlate them with their role in the PT constitutes the main purpose of this work.

In contrast to the experiments on tropolone derivatives in which the electronic spectroscopies such as fluorescence excitation and hole-burning are measured and the PT is identified *via* its effects on certain collective normal modes [28–34], this work examines the PT motion on the electronic ground state surface which is accessible by ultrafast mid-IR vibrational spectroscopy [35–37] directly. More specifically, the reactive proton's (x, y) coordinates in the 3CTR molecular plane will be chosen as the reduced reaction system. The remaining substrate Cartesian coordinates, including the proton's z-coordinate, will be transformed into a set of normal modes with reference to a chosen molecular configuration and considered as the bath. Mode mixing will occur for the substrate as the molecule deviates from the reference configuration. The quantum chemical construction of the all-Cartesian system-plus-substrate Hamiltonian will be outlined in Section 2. The resulting total Hamiltonian in a reduced dynamics description will then be partitioned into coherent (deterministic) and incoherent (stochastic) parts. The former which is also called the *reduced reaction Hamiltonian* will be detailed in Section 3. It consists of the bare reaction Hamiltonian, the substrate's (bath) reorganization energy which effectively leads to the minimum energy reaction path, and the bath thermal ensemble average of the system-substrate interaction which is temperature-dependent. The incoherent or stochastic system-substrate coupling will be described in Section 4 in terms of the substrate's interaction spectra. As the coupling is considered up to the second order in the substrate DOF, the interaction spectra will be analyzed in terms of the one-phonon and two-phonon coupling strengths for individual substrate modes. Using quantum dissipation theory as outlined in Appendix A, the effects of incoherent system-substrate interaction will further be expressed in terms of Bloch's state-to-state T_1-relaxation and *pure* T_2-dephasing rates in Section 5. By virtue of the quantum chemical CRH construction, we can establish the correlation between the *molecular patterns* of the dominant substrate normal modes and their role for the T_1-relaxation and the pure T_2-dephasing, thereby distinguishing *inter-well* and *intra-well* processes.

2 Quantum chemical construction of a system-plus-substrate Hamiltonian

2.1 General formulation

Consider an intramolecular PT reaction in a large polyatomic molecule. Here, the separation between system DOF and substrate modes is intuitively clear since only a specific proton performs large amplitude anharmonic motions; the other atoms/modes are well approximated in terms of harmonic oscillators [9] and can be treated as a bath in the reduced description as will be shown subsequently. Let us denote the Cartesian coordinates for the reactive and the substrate modes in terms of vectors $\mathbf{X}$ and $\mathbf{Q}$, containing N_r and $3N - N_r$ elements, respectively. Here, N is the number of atoms in the molecule.

The all-Cartesian system-plus-substrate PES is defined by the first terms of a Taylor expansion with respect to small deviations of the substrate coordinates at a given value of the reaction coordinate [7]

$$U(\mathbf{X};\mathbf{Q}) \approx U_0(\mathbf{X}) + \mathbf{U}_1^{\mathrm{T}}(\mathbf{X})\delta\mathbf{Q} + \frac{1}{2}\delta\mathbf{Q}^{\mathrm{T}}\mathbf{U}_2(\mathbf{X})\delta\mathbf{Q}. \quad (1)$$

Here, the superscript T denotes the transpose, $\delta\mathbf{Q} \equiv \mathbf{Q} - \mathbf{Q}_0$ with $\mathbf{Q}_0$ being the reference substrate configuration that will be specified later, and $U_0(\mathbf{X}) \equiv U(\mathbf{X};\mathbf{Q}_0)$. The (force) vector $\mathbf{U}_1$ and the (Hessian) symmetric matrix $\mathbf{U}_2$ are, respectively, the first- and the second-order derivatives of $U(\mathbf{X};\mathbf{Q})$ with respect to $\mathbf{Q}$ and evaluated at the chosen $\mathbf{Q}_0$. Note that equation (1) in general does not conserve the total angular and linear momenta of the molecule [3].

The construction of the all-Cartesian PES $U(\mathbf{X};\mathbf{Q})$ [Eq. (1)] involves the following steps:

(i) quantum chemical determination of the minima and the saddle points on the PES. They amount to the reactant, the product, and the transition state configurations and will be used to identify suitable reaction $\mathbf{X}$ and substrate $\mathbf{Q}$ coordinates. One of the stationary configurations is chosen as the reference $\{\mathbf{X}_0;\mathbf{Q}_0\}$ for both the reaction and substrate coordinates;

(ii) evaluation of the PES $U(\mathbf{X};\mathbf{Q})$ [Eq. (1)] in terms of $\{U_0(\mathbf{X}), \mathbf{U}_1(\mathbf{X}), \mathbf{U}_2(\mathbf{X})\}$ at each point on a specified N_r-dimensional $\mathbf{X}$-grid with the chosen reference substrate configuration $\mathbf{Q}_0$;

(iii) transformation of the substrate Cartesian coordinate $\mathbf{Q}$ to the normal mode coordinates $\mathbf{q} \equiv \mathbf{S}^{-1}\delta\mathbf{Q}$ with respect to a reference value of the reaction coordinate $\mathbf{X}_{\mathrm{ref}}$, which in principle can be arbitrary [7].

In this work $\mathbf{X}_{\mathrm{ref}}$ is set to be equal to $\mathbf{X}_0$. The effect of different choices for $\mathbf{X}_{\mathrm{ref}}$ and the more elaborated flexible substrate reference [7] in which $\mathbf{Q}_0 = \mathbf{Q}_0(\mathbf{X})$ depends in the system coordinates will be discussed in Section 6 and investigated elsewhere.

To proceed, let us denote

$$\mathbf{F}(\mathbf{X}) \equiv \mathbf{S}^{\mathrm{T}}\mathbf{U}_1(\mathbf{X}), \quad (2)$$

$$\mathbf{G}(\mathbf{X}) \equiv \mathbf{S}^{\mathrm{T}}[\mathbf{U}_2(\mathbf{X}) - \mathbf{U}_2(\mathbf{X}_0)]\mathbf{S}. \quad (3)$$

Notice that the transformation matrix $\mathbf{S}$ defines the normal modes of the substrate at $\mathbf{X}_0$ only, *i.e.*

$$\mathbf{U}'' \equiv \mathbf{S}^{\mathrm{T}}\mathbf{U}_2(\mathbf{X}_0)\mathbf{S} \equiv \mathrm{diag}(\omega_1^2, \omega_2^2, ...), \quad (4)$$

is diagonal and positive. Here, ω_j is the substrate normal mode frequency when the reaction coordinate is at $\mathbf{X}_0$. Since the chosen reference coordinate $\mathbf{X}_0$ is a stationary point, we have $\mathbf{U}_1(\mathbf{X}_0) = \mathbf{F}(\mathbf{X}_0) = \mathbf{0}$. In general, at other values of $\mathbf{X}$, $\mathbf{F}(\mathbf{X}) \neq \mathbf{0}$ and $\mathbf{G}(\mathbf{X})$ is non-diagonal.

To avoid the non-physical mixing of the substrate's low frequency vibrations and the molecule's overall motions, we shall further project out the six DOF for translations and rotations. This can be done, as suggested in references [3,7], by considering infinitesimal overall rotations and translations. By doing this we neglect the effects of rotation-vibration coupling which is reasonable in view of the application to the PT in a large molecule.

Table 1. Relative energies, dipole moments and some geometrical parameters of the two isomers (E1 and E2) and the transition state (TS) of 3CTR calculated by the DFT/B3LYP method using a 6-31+G(d, p) basis set. Values within parentheses are results from a MP2/6-31+G(d, p) calculation.

	E1	TS	E2
E (cm^{-1})	0(0)	1875(2044)	258(275)
$\lvert\mu\rvert$ (Debye)	4.55(5.56)	4.74(5.92)	4.12(5.06)
$r_{\mathrm{HO_1}}$ (Å)	1.80(1.82)	1.22(1.22)	0.99(0.99)
$r_{\mathrm{HO_2}}$ (Å)	0.99(0.99)	1.24(1.24)	1.78(1.80)
$r_{\mathrm{O_1C_1}}$ (Å)	1.25(1.26)	1.29(1.30)	1.33(1.34)
$r_{\mathrm{O_2C_2}}$ (Å)	1.34(1.34)	1.29(1.30)	1.25(1.27)
$r_{\mathrm{O_1O_2}}$ (Å)	2.49(2.50)	2.30(2.31)	2.48(2.50)

The correlated system-plus-substrate CRH thus assumes the form

$$H_{\mathrm{T}} = H_0 + h_{\mathrm{B}} + H_{\mathrm{SB}}, \quad (5)$$

$$H_0 = \sum_{n=1}^{N_r} \frac{P_n^2}{2M_n} + U_0(\mathbf{X}), \quad (6)$$

$$h_{\mathrm{B}} = \frac{1}{2}\sum_{j=1}^{N'}(p_j^2 + \omega_j^2 q_j^2), \quad (7)$$

$$H_{\mathrm{SB}} = \mathbf{F}^{\mathrm{T}}(\mathbf{X})\mathbf{q} + \frac{1}{2}\mathbf{q}^{\mathrm{T}}\mathbf{G}(\mathbf{X})\mathbf{q}. \quad (8)$$

Here, N_r and $N' = 3N - N_r - 6$ are the number of DOF of the reaction coordinates ($\mathbf{X}$) and the harmonic substrate ($\mathbf{q}$), respectively.

2.2 Application to proton transfer in 3-chlorotropolone

We are now in the position to apply the CRH approach to the intramolecular PT in 3CTR, *cf.* Figure 1. First, the quantum chemical geometry optimization was carried out using the DFT(B3LYP)/6-31+G(d, p) and the MP2/6-31+G(d, p) method. Both predict planar structures for the two stable isomers and the transition state of the PT reaction. The relative energies, dipole moments and some geometrical parameters of the stationary configurations are listed in Table 1. Obviously, the less expensive density functional calculation reproduces the MP2 results reasonably well. All calculations are performed using Gaussian98 [38].

The reaction coordinate is chosen as $\mathbf{X} = (x, y)$ for the position of the reactive H atom in the molecular plane. Here, the x-axis is directed from O_1 at 70° to the bond O_1–C_1 (Gaussian98 standard orientation, *cf.* Fig. 1). We use the most stable configuration E1 (*cf.* Fig. 1) as the reference $\mathbf{X}_0 = (x_0, y_0)$ and also for defining $\mathbf{Q}_0$. The CRH [Eqs. (5–8)] is determined with the DFT/B3LYP method

and the Hessian is calculated on the Hartree-Fock level of theory. The normal modes of the substrate are defined for the reference configuration (x_0, y_0) of E1 (*cf.* Fig. 1) and their frequencies are calculated according to equation (4). In the present application, the number of atoms in 3CTR is $N = 15$, *i.e.* the number of DOF is $N_r = 2$ for the reaction coordinate and $N' = 37$ for the substrate. The mass in equation (6) is that of the proton, $M_n = M_{\rm H}$.

In the following, we adopt a Bloch-Redfield type of reduced description to the PT in 3CTR as outlined in Appendix A. Here, the $N' = 37$ substrate modes are treated as the intramolecular bath that is assumed to be Markovian. In the reduced description we need to identify the effective or reduced reaction Hamiltonian H [*cf.* Eq. (34)] and the Redfield tensor $\mathcal{R}$ [Eq. (36)]. The former governs the coherent PT dynamics, while the latter controls dissipation induced *via* the system-substrate interaction which is treated as a stochastic variable. The reduced reaction Hamiltonian H will be specified in Section 3 in terms of the bare reaction Hamiltonian [Eq. (6)], the substrate-bath reorganization energy which effectively leads to the minimum energy reaction path, and the thermal ensemble average of system-substrate interaction. The dynamical effects of system-substrate coupling will be first treated in Section 4 in terms of the substrate's interaction spectra, and then in Section 5 in terms of their induced state-to-state T_1-relaxation and pure T_2-dephasing rates. The substrate normal modes and their interaction with the PT reaction system will be analyzed on a molecular level.

3 Effective reaction system Hamiltonian

In a reduced description, the effective reaction Hamiltonian in the presence of a substrate (bath) is not equal to the bare potential H_0 [Eq. (6)], but we have

$$H = \sum_{n=1}^{N_r} \frac{P_n^2}{2M_n} + V(\mathbf{X}), \tag{9}$$

with the effective potential given by

$$V(\mathbf{X}) = U_0(\mathbf{X}) + V_{\rm reor}(\mathbf{X}) + \langle H_{\rm SB}\rangle \cdot \tag{10}$$

Here, $U_0(\mathbf{X})$ is the bare potential [*cf.* Eq. (6)], while $V_{\rm reor}(\mathbf{X})$ is the reorganization energy that compensates the energy renormalization induced by $H_{\rm SB}$ [Eq. (8)]. It can be shown that in certain well-defined limits such as high-temperature or Markovian regime [23,40,41], the effects of the second-order system-bath correction on both the canonical thermal equilibrium and the reduced dynamics may be accounted for by the Caldeira-Leggett form of $V_{\rm reor}$. The expression for $V_{\rm reor}$ can be obtained by finding the minimum of the system-plus-substrate potential for a given $\mathbf{X}$, that is [23]

$$V_{\rm reor}(\mathbf{X}) = -\frac{1}{2}\mathbf{F}^{\rm T}(\mathbf{X})[\mathbf{G}(\mathbf{X}) + \mathbf{U}'']^{-1}\mathbf{F}(\mathbf{X}). \tag{11}$$

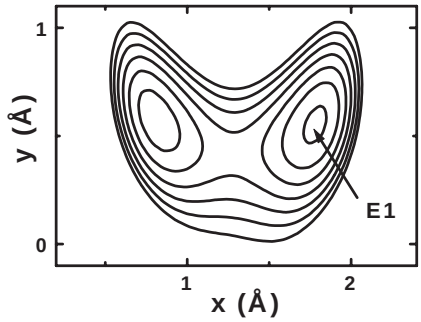

Fig. 2. The effective PES $V(x, y)$ [Eq. (10)] at $T = 200$ K for the PT reaction of 3CTR for the reference configuration being set to E1 (*cf.* Fig. 1). The contour lines go from 0 to 10 000 cm^{-1}.

In equation (10), $\langle H_{\rm SB}\rangle$ denotes the contribution of the substrate ensemble average of $H_{\rm SB}$ [Eq. (8)]. This term enters the effective Hamiltonian in first order perturbation theory (mean field term) [24]. It reads ($\hbar \equiv 1$)

$$\langle H_{\rm SB}\rangle \equiv {\rm Tr}_{\rm B}[H_{\rm SB}\rho_{\rm B}^{\rm eq}(T)] = \frac{1}{2}\sum_{j,k} G_{jk}(\mathbf{X})\langle q_j q_k\rangle$$
$$= \sum_{j=1}^{N'} \frac{G_{jj}(\mathbf{X})}{2\omega_j}\left(\bar{n}_j + \frac{1}{2}\right)\cdot \tag{12}$$

Here, $\rho_{\rm B}^{\rm eq}(T) = {\rm e}^{-\beta h_{\rm B}}/{\rm tr}_{\rm B}{\rm e}^{-\beta h_{\rm B}}$; with $\beta = 1/(k_{\rm B}T)$, is the canonical thermal ensemble density operator of the harmonic substrate [Eq. (7)], and

$$\bar{n}_j = [\exp(\beta\omega_j) - 1]^{-1}, \tag{13}$$

is the thermal occupation number of the jth harmonic substrate mode. In deriving equation (12), we used the identities $\langle q_j\rangle = 0$ and $\langle q_j q_k\rangle = \omega_j^{-1}(\bar{n}_j + 1/2)\delta_{jk}$ for the independent harmonic substrate (bath) model [Eq. (7)]. Note that $\langle H_{\rm SB}\rangle$, and hence, $V(\mathbf{X})$ and H are temperature dependent. In case of the linear coupling approximation: $\mathbf{G}(\mathbf{X}) = 0$, equation (12) is zero and equation (11) reduces to the standard Caldeira-Leggett form of reorganization energy [23,39].

Figure 2 shows the quantum chemically constructed (*cf.* Sect. 2) effective (or reduced) PES, $V(\mathbf{X}) \equiv V(x, y)$ [Eq. (10)] at $T = 200$ K for the PT reaction of 3CTR. Note that at the reference E1 configuration $\mathbf{X}_0 = (x_0, y_0)$ (*cf.* Fig. 1) $V(x_0, y_0) = U_0(x_0, y_0)$ is independent of temperature and will be used to define the zero of energy.

In Figure 3 we plotted a cut through the effective PES along the x-direction and at $y = y_0$ for different temperatures [$T = 200$ K (solid curve), $T = 0$ K (dotted curve) and 400 K (dashed curve)]. It can be seen that the reduced system potential barrier height is enhanced as the temperature increases. This may be considered as a hint that as the incoherent substrate motion increases, the coherent PT rate is effectively reduced.

In Figure 4 we show the energies of the five lowest vibrational eigenstates ε_a of equation (9) as a function of temperature. The corresponding eigenfunctions at

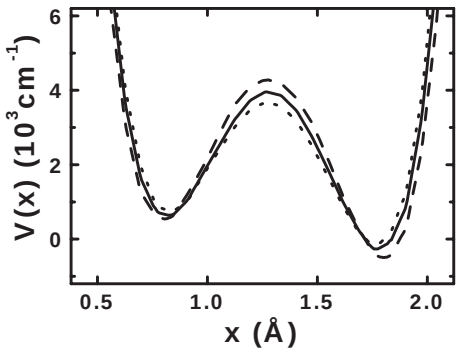

Fig. 3. The reaction path projected from the PES $V(x, y)$ (*cf.* Fig. 2) onto the x-coordinate for $y = y_0$ at 0 K (dotted line), 200 K (solid line) and 400 K (dashed line).

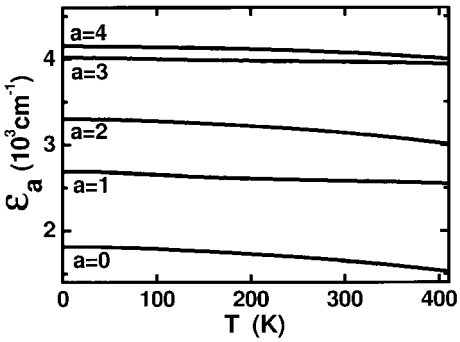

Fig. 4. The five lowest vibrational eigenenergies ε_a of the reduced reaction system [Eq. (9)] as functions of temperature.

$T = 200$ K are given in Figure 5. The diagonalization of the reduced reaction Hamiltonian H [Eq. (9)] was carried out using the DVR method [42,43]. It is evident that $\{|0\rangle, |2\rangle, |4\rangle\}$ are localized mostly in the E1-potential well, while $\{|1\rangle, |3\rangle\}$ are mostly localized in the E2-potential well.

At this point it should be noted that the significance of the eigenstates shown in Figures 4 and 5 depends on a number of factors. PT reactions are often described in two limits [24]: in the adiabatic case the proton is moving and the substrate atoms can adjust to the proton's position instantaneously, *i.e.* they relax to the respective minimum energy configuration. In the frozen substrate limit only the proton is moving while the substrate is fixed, *e.g.*, at the most stable configuration. In the present case $U_0(x, y)$ corresponds to the frozen substrate potential while $V(x, y)$ – apart from the mean field term – describes the adiabatic case. In other words, the reorganization energy is just the energy which is required to relax the substrate atoms to the equilibrium configuration according to the actual value of (x, y). Therefore, the eigenstates of H are in accord with the assumption one usually does for the adiabatic limit of PT. Going beyond this limit would imply that the excitation of the substrate modes is explicitly taken into account, *i.e.* the present eigenstates would in principle mix with the vibrational excitations of the substrate modes. In the following section we follow a different strategy and account for the interaction with the substrate

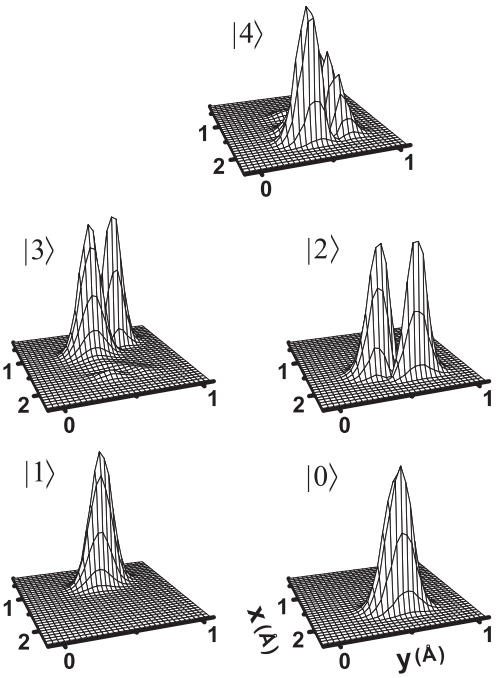

Fig. 5. The five lowest localized vibrational eigenstates of equation (9) at 200 K.

by using second order perturbation theory. Finally, it must be emphasized that our reasoning, of course, relies on the validity of the harmonic approximation for the substrate atoms for all values of the reaction coordinate. Intuitively, one expects that anharmonicities become the more important the farther one moves away from the fixed reference point (x_0, y_0). Thus the energies and rates calculated below which are related to the states localized close to E1, $\{|0\rangle, |2\rangle, |4\rangle\}$ will be more reliable than those referring to states $\{|1\rangle, |3\rangle\}$. In principle this limitation can be overcome by using substrate atom configurations for the calculation of the forces and the Hessian which are adapted to the actual position of the proton [7]. Respective work for tropolone derivatives is in progress in our groups.

4 Substrate interaction spectra

4.1 Stochastic model

The dynamics of the reaction subsystem is not only governed by the reduced effective reaction Hamiltonian [Eq. (9)], but also influenced by the system-substrate interaction. For a large polyatomic molecule, the substrate has many DOF ($\mathbf{q}$) and may be approximated as a dissipative bath. The system-bath interaction, after removing the thermal bath ensemble average, is [*cf.* Eqs. (8, 12)]

$$H' \equiv H_{\mathrm{SB}} - \langle H_{\mathrm{SB}} \rangle = \sum_j F_j(\mathbf{X}) q_j + \frac{1}{2} \sum_{j,k} G_{jk}(\mathbf{X}) [q_j q_k - \langle q_j q_k \rangle]. \quad (14)$$

Here, $F_j(\mathbf{X})$ and $G_{jk}(\mathbf{X})$ denote the elements of the vector $\mathbf{F}(\mathbf{X})$ and matrix $\mathbf{G}(\mathbf{X})$, respectively. Within second order perturbation theory the effect of the system-substrate

interaction on the reaction dynamics is accounted for by the correlation function

$$\langle H'(t)H'(0)\rangle \equiv \langle \mathrm{e}^{\mathrm{i}h_{\mathrm{B}}t}H'\mathrm{e}^{-\mathrm{i}h_{\mathrm{B}}t}H'\rangle. \tag{15}$$

The above equation also defines $H'(t)$ as a stationary stochastic operator *via* its dependence on the substrate modes, $\mathbf{q}(t) = \mathrm{e}^{\mathrm{i}h_{\mathrm{B}}t}\mathbf{q}\mathrm{e}^{-\mathrm{i}h_{\mathrm{B}}t}$. Here, h_{B} is the substrate Hamiltonian [Eq. (7)].

In order to obtain a suitable form of H' let us introduce the dimensionless polynomial operator in the reaction coordinate $\mathbf{X} = (x, y)$ space

$$W_\alpha \equiv (M_{\mathrm{H}}\omega_0)^{(\alpha_x+\alpha_y)/2}(x-x_0)^{\alpha_x}(y-y_0)^{\alpha_y} \tag{16}$$

with $\alpha \equiv (\alpha_x, \alpha_y)$ and $\alpha_x, \alpha_y = 0, 1, ...$ Here, M_{H} is the proton mass and ω_0 a frequency scaling parameter which is set to 1 500 cm^{-1}, *i.e.* about the transition frequency ω_{20}. Using this expansion we have

$$F_j(\mathbf{X}) \equiv \sum_\alpha f_{\alpha j}W_\alpha, \tag{17}$$

$$G_{jk}(\mathbf{X}) \equiv \sum_\alpha g_{\alpha jk}W_\alpha. \tag{18}$$

We can thus express H' [Eq. (14)] in the following form:

$$H' \equiv \sum_\alpha W_\alpha\phi_\alpha, \tag{19}$$

with the generalized Langevin force given by

$$\phi_\alpha \equiv \sum_j f_{\alpha j}q_j + \frac{1}{2}\sum_{j,k} g_{\alpha jk}[q_jq_k - \langle q_jq_k\rangle]\cdot \tag{20}$$

and $\langle q_jq_k\rangle = \omega_j^{-1}(\bar{n}_j + 1/2)\delta_{jk}$. The parameters $f_{\alpha j}$ and $g_{\alpha jk}$ defined in equations (17, 18) can readily be determined from the quantum chemistry calculation of Section 2. Note that in the case of $\alpha = (0, 0)$, we have $f_{\alpha j} = 0$ and $g_{\alpha jk} = 0$.

4.2 Interaction spectra and coupling strengths

The effect of the bath (substrate) on the reduced reaction dynamics can be expressed in terms of the bath interaction spectra $C_{\alpha\alpha'}(\omega)$ [*cf.* Eq. (35)], which are defined as the Fourier transform of the Langevin force-force correlation function:

$$C_{\alpha\alpha'}(\omega) \equiv \int_{-\infty}^{\infty}\mathrm{d}t\,\mathrm{e}^{\mathrm{i}\omega t}\langle\phi_\alpha(t)\phi_{\alpha'}(0)\rangle\cdot \tag{21}$$

Note that in the present notation [*cf.* Eqs. (16, 19)] both $C_{\alpha\alpha'}$ and ϕ_α have units of a frequency. It can be shown easily that $C_{\alpha\alpha'}(\omega)$ is real and if $\alpha = \alpha'$, it's positive as well. Further the detailed-balance condition holds:

$$C_{\alpha'\alpha}(-\omega) = \mathrm{e}^{-\beta\omega}C_{\alpha\alpha'}(\omega). \tag{22}$$

As the generalized Langevin force ϕ_α [Eq. (20)] contains both, linear and quadratic terms in the substrate modes, we can express $C_{\alpha\alpha'}(\omega)$ as the sum of its one-phonon $C^{(1)}_{\alpha\alpha'}$ and two-phonon contributions. For the latter one can distinguish the so-called pump-pump $C^{(+)}_{\alpha\alpha'}$ and pump-dump $C^{(-)}_{\alpha\alpha'}$ components. Thus we have

$$C_{\alpha\alpha'}(\omega) = C^{(1)}_{\alpha\alpha'}(\omega) + C^{(+)}_{\alpha\alpha'}(\omega) + C^{(-)}_{\alpha\alpha'}(\omega). \tag{23}$$

By using equations (20, 21), together with some elementary algebra for independent harmonic oscillators we obtain

$$C^{(1)}_{\alpha\alpha'}(\omega) = \sum_j A_{\alpha\alpha'}(j)[(\bar{n}_j+1)\delta(\omega-\omega_j) + \bar{n}_j\delta(\omega+\omega_j)], \tag{24}$$

and

$$C^{(+)}_{\alpha\alpha'}(\omega) = \sum_{jk} B_{\alpha\alpha'}(j,k)[\bar{n}_j\bar{n}_k\delta(\omega+\omega_j+\omega_k) + (\bar{n}_j+1)(\bar{n}_k+1)\delta(\omega-\omega_j-\omega_k)]\ , \tag{25}$$

$$C^{(-)}_{\alpha\alpha'}(\omega) = 2\sum_{jk} B_{\alpha\alpha'}(j,k)(\bar{n}_j+1)\bar{n}_k\delta(\omega-\omega_j+\omega_k). \tag{26}$$

Here,

$$A_{\alpha\alpha'}(j) = \pi f_{\alpha j}f_{\alpha' j}/\omega_j, \tag{27}$$

and

$$B_{\alpha\alpha'}(j,k) = \pi g_{\alpha jk}g_{\alpha' jk}/(4\omega_j\omega_k). \tag{28}$$

In the present notation both the one-phonon and the two-phonon coupling strengths, $A_{\alpha\alpha'}(j)$ and $B_{\alpha\alpha'}(j,k)$, have units of a frequency squared. They measure the specific bath mode(s) coupling with the reduced PT system. The two-phonon coefficient $B_{\alpha\alpha'}(j,k)$ [Eq. (28)] also describes the substrate mode-mixing (for $j \neq k$) and frequency change (for $j = k$) as a consequence of the PT process (*i.e.*, away from the reference configuration E1). Obviously, $A^2_{\alpha\alpha'}(j) = A_{\alpha\alpha}(j)A_{\alpha'\alpha'}(j)$ and $B^2_{\alpha\alpha'}(j,k) = B_{\alpha\alpha}(j,k)$ $B_{\alpha'\alpha'}(j,k)$. The index $\alpha \equiv (\alpha_x, \alpha_y)$ determines the order of the system coordinate operator [*cf.* Eq. (16)]. In the following the expansion in equation (16) has been restricted to terms for which $\alpha_x+\alpha_y \leq 2$. For the interaction strength one observes that the $A_{\alpha\alpha}$ or $B_{\alpha\alpha}$ with $\alpha = (1, 0)$ and $(0, 1)$ are usually larger than those with $\alpha = (2, 0)$, $(1, 1)$ and $(0, 2)$.

In Table 2 we have listed the frequencies ω_j, one-phonon coupling strengths $A_{\alpha\alpha}(j)$ [Eq. (27)], and degenerate two-phonon coupling strengths $B_{\alpha\alpha}(j,j)$ [Eq. (28)] for each of the 37 substrate normal modes. The non-degenerate two-phonon coefficients $B_{\alpha\alpha}(j,k)$ with $j \neq k$ are overall smaller than the degenerate ones and are not shown here. It is convenient to arrange the substrate vibrations into *in-plane* and *out-of-plane* modes. They are presented in the upper and the lower parts of Table 2, respectively.

Table 2. Substrate normal mode frequencies ω_j and coupling strengths $A_{\alpha\alpha}(j)$ and $B_{\alpha\alpha}(j,j)$ [Eqs. (27, 28)]. The upper/lower part shows the in-plane/out-of-plane modes. The strongest coupled modes shown in Figures 6–8 are highlighted.

j	ω_j	$A_{\alpha\alpha}(j)$ (cm^{-2})					$B_{\alpha\alpha}(j,j)$ (cm^{-2})				
	(cm^{-1})	$\alpha=(1,0)$	$(0,1)$	$(2,0)$	$(1,1)$	$(0,2)$	$\alpha=(1,0)$	$(0,1)$	$(2,0)$	$(1,1)$	$(0,2)$
1	3202	0.66	0.11	0.36	0.022	0.085	0.075	0.028	0.0	0.0	0.0
2	3193	2.6	14	0.62	0.053	1.7	0.84	0.030	0.002	0.003	0.0
3	3185	11	19	0.40	0.17	0.14	0.81	0.026	0.0	0.0	0.0
4	3175	66	55	0.060	1.2	0.75	0.062	0.037	0.0	0.001	0.0
5	1652	3.1×10^4	7100	630	1.1×10^4	520	1.6	70	0.15	0.85	0.078
6	1643	7300	6.3×10^4	3200	4700	2.1×10^4	35	6.7	0.36	1.6	0.35
7	1609	3.8×10^5	9.2×10^4	2200	1.1×10^4	1.3×10^4	84	22	1.6	4.2	1.7
8	1514	3.0×10^5	1.7×10^5	260	2.3×10^4	13	130	60	5.1	0.010	1.3
9	1506	1.9×10^5	8.5×10^4	2800	2000	3600	2.3	2.8	0.008	0.096	0.058
10	1425	5.3×10^5	3.1×10^5	4900	7400	1.0×10^4	130	6.8	0.018	0.21	1.0
11	1382	8.8×10^4	8.6×10^4	2700	8900	490	34	41	0.24	1.3	0.044
12	1343	1.4×10^5	1.3×10^5	7800	1900	62	230	11	0.18	1.6	32
13	1264	2.1×10^4	3.5×10^4	530	7400	1800	28	1.2	0.0	0.21	3.1
14	1239	1500	1.0×10^5	1100	1.7×10^4	9700	0.41	0.0	0.073	0.33	0.11
15	1129	5.4×10^4	1.9×10^5	710	4.5×10^4	1.6×10^4	160	180	1.9	5.7	3.9
16	1028	7.0×10^5	5.5×10^5	1.6×10^4	4100	1700	530	380	8.0	15	0.89
17	934	4.3×10^5	7.7×10^5	4000	2.1×10^4	2.7×10^4	930	1100	12	50	24
18	**865**	1.4×10^8	2.3×10^8	2.1×10^6	6.6×10^6	6.1×10^6	1.3×10^5	9.3×10^4	2100	3500	770
19	820	3.5×10^5	7.4×10^5	11	9.1×10^4	5.7×10^4	1500	2300	20	120	98
20	735	8.7×10^4	4.0×10^4	280	4 90	4.6×10^4	0.079	30	0.048	5.5	0.093
21	551	5.3×10^5	6.2×10^5	3.2×10^4	7300	4600	1.6×10^4	0.30	1400	1600	1.0
22	539	6.6×10^4	2000	2.8×10^4	1.9×10^5	6.0×10^4	200	33	8.0	0.60	0.38
23	402	1.5×10^5	7.7×10^5	2000	6.8×10^4	1.1×10^4	100	110	2.3	0.33	18
24	339	2800	1.5×10^5	1.9	6500	1400	7.4	35	3.9	26	2.0
25	**273**	1.9×10^5	1.8×10^5	5.7×10^4	1.1×10^5	1.5×10^5	3.1×10^4	1600	2500	1000	220
26	1013	0.27	0.45	0.004	0.017	0.011	4.5	0.93	0.018	0.0	0.047
27	980	0.19	0.36	0.002	0.017	0.011	7.8	0.18	0.065	0.010	0.043
28	912	0.20	0.35	0.003	0.009	0.010	82	120	5.0	1.0	9.3
29	**803**	0.008	0.015	0.0	0.0	0.0	8.0×10^6	5.2×10^6	2.1×10^5	1.0×10^5	2.1×10^5
30	**764**	0.43	0.70	0.005	0.019	0.030	7.2×10^4	4.6×10^4	1800	1100	2000
31	760	0.037	0.066	0.0	0.002	0.003	39	2.7	2.1	2.4	1.0
32	597	0.040	0.10	0.0	0.013	0.009	260	150	2.6	2.1	8.8
33	494	0.029	0.068	0.0	0.003	0.003	430	330	7.2	0.003	21
34	378	0.004	0.002	0.0	0.0	0.002	180	240	8.6	0.65	15
35	256	0.015	0.16	0.001	0.057	0.004	360	580	11	6.0	43
36	**139**	0.001	0.008	0.0	0.002	0.0	1.2×10^4	62	650	1000	23
37	**84**	0.0	0.001	0.0	0.0	0.0	1.3×10^5	1.3×10^4	4200	510	960

Some details of Table 2 are worth emphasizing: first, the first four in-plane and the first two out-of-plane modes involve largely the motions of non-reactive H atoms such as CH stretching vibrations. They are of high frequencies and rather *localized*. Thus these six localized modes have rather small values of $A_{\alpha\alpha}$ and $B_{\alpha\alpha}$. Second, the modes $j = 18$ and 25 are of relatively large overall coupling strengths among those of the in-plane type. In fact the mode $j = 18$ has the strongest coupling strengths among all the 37 substrate modes. As depicted in Figure 6, these two important in-plane modes ($j = 18$ and 25) involve relatively large bending motion of the two oxygen atoms which *promotes* the PT. Third, the modes $j = 29$, 30, 36 and 37 are of relative large coupling strengths among those of the out-of-plane type. The former two are shown in Figure 7 and involve large amplitudes for the motion of the reactive proton along the z-direction (out-of-plane bending type). The latter two are shown in Figure 8 and involve the out-of-plane motion of the two oxygen atoms in opposite directions.

Table 2 reveals also some general trends: it is observed that with a few exceptions, $A_{\alpha\alpha}(j) > B_{\alpha\alpha}(j,j)$ for the

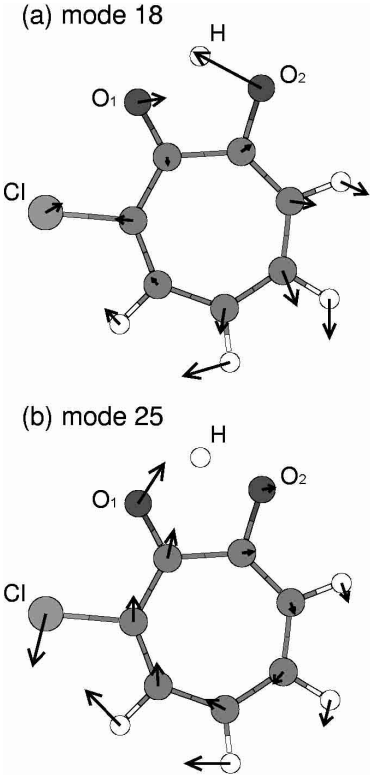

Fig. 6. The in-plane substrate normal modes for (a) $j = 18$ and (b) $j = 25$.

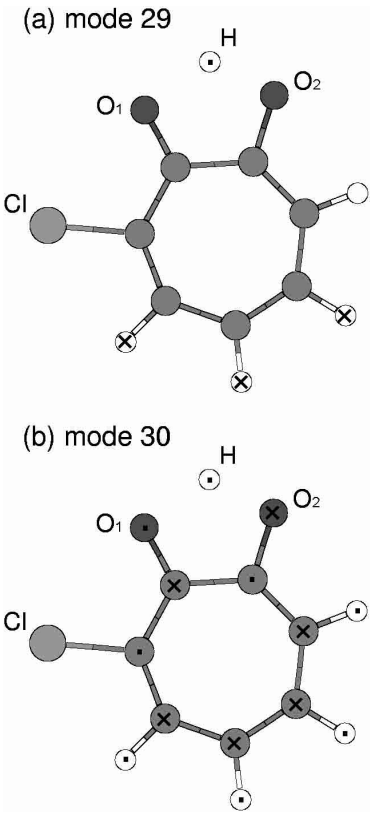

Fig. 7. The out-of-plane substrate normal modes for (a) $j = 29$ and (b) $j = 30$.

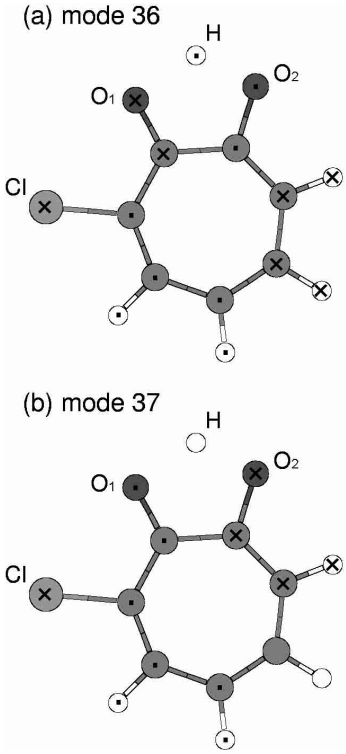

Fig. 8. The out-of-plane substrate normal modes for (a) $j = 36$ and (b) $j = 37$.

in-plane modes, while $A_{\alpha\alpha}(j) < B_{\alpha\alpha}(j,j)$ for out-of-plane modes. Overall it is found that the in-plane one-phonon coupling strengths $\{A_{\alpha\alpha}\}$ are much larger than their out-of-plane counterparts while the two-phonon coupling strengths $\{B_{\alpha\alpha}\}$ are much less sensitive to the character of the substrate modes. This behavior can be traced back to the fact that the PT is essentially an in-plane motion and in particular the stable states are planar. Therefore, for a fixed reference geometry the forces exerted on the substrate upon proton motion will mostly act to distort the geometry in the plane of the molecule. On the other hand, it is well-known that the frequency, for instance, of the out-of-plane bending vibration with respect to the hydrogen bond changes considerably during PT. In the present case we have for the stationary points on the fully relaxed potential surface: $\omega_{\text{bend}} = 812\ \text{cm}^{-1}$ (E1), $\omega_{\text{bend}} = 1\,235\ \text{cm}^{-1}$ (TS), and $\omega_{\text{bend}} = 835\ \text{cm}^{-1}$ (E2). Thus it is to be expected that the modes with out-of-plane bending character, such as mode 29, have the strongest quadratic coupling strength.

In the next section, the most important in-plane and out-of-plane substrate modes shown in Figures 6–8 will further be examined in terms of their implications for the state-to-state T_1-relaxation and pure T_2-dephasing rates in the reduced description of the PT. We will demonstrate that while both the one-phonon parameter $A_{\alpha\alpha}$ and the two-phonon parameter $B_{\alpha\alpha}$ are responsible for the T_1-relaxation, only the latter plays an important role in determining the pure T_2-dephasing dynamics if the temperature is not too low.

Obviously, for the substrate interaction spectra [*cf.* Eqs. (23–28)] the effect of a specific substrate mode on the PT system depends not only on $A_{\alpha\alpha}(j)$ and $B_{\alpha\alpha}(j,j)$, but also on the thermal occupation number $\bar{n}_j$. Furthermore, the delta-functions in equations (24–26) should be understood as certain line shape functions of finite widths, induced, for example, *via* rotational motion. In this work, we use a simple Lorentz line shape with a width of 2 cm^{-1} to replace each of the δ-functions in equations (24–26) in the positive frequency ($\omega > 0$) domain. The obtained $C_{\alpha\alpha'}(\omega > 0)$ is then used to construct $C_{\alpha\alpha'}(\omega < 0)$ employing the detailed-balance relation (Eq. (22)).

5 T_1-relaxation and T_2-dephasing

5.1 General remarks

So far we have discussed the various bath (substrate) modes in terms of their coupling strengths $A_{\alpha\alpha'}(j)$ [Eq. (27)] and $B_{\alpha\alpha'}(j,k)$ [Eq. (28)] and their contribution to the system-substrate interaction spectra. In this section, we shall discuss their relevance in terms of the phase and energy relaxation dynamics. In the Markovian limit, the substrate interaction spectra evaluated in the previous section can in principle be used to construct the complete Redfield dissipation tensor $\mathcal{R}$ (*cf.* Appendix A) which accounts for the effect of incoherent substrate interaction on the PT in the reduced space [44–46].

In the following we will restrict the discussion to the case of the Bloch approximation [Eq. (38)] where only the secular terms $\mathcal{R}_{aa,bb}$ and $\mathcal{R}_{ab,ab}$ are retained. They have a straightforward interpretation in terms of T_1-relaxation and the T_2-dephasing rates, respectively [44,47,48]. Thus, we provide a benchmark calculation of the T_1- and T_2-rates based on the quantum chemical construction of the system-plus-substrate Hamiltonian as described in the previous section.

5.2 Formulation of T_1- and T_2-rate constants

Let us start with the state-to-state T_1-relaxation rate for the $a \leftarrow b$ transition ($a \neq b$) denoted as $\gamma_1^{ab} \equiv -\mathcal{R}_{aa,bb}$. Here, a and b are two vibrational eigenstates of the reduced reaction system Hamiltonian H [Eq. (9)]. By using equation (36), we obtain [46]

$$\gamma_1^{ab} = \sum_{\alpha\alpha'} C_{\alpha\alpha'}(\omega_{ba}^{\mathrm{S}}) W_\alpha^{ba} W_{\alpha'}^{ab}\,; \qquad \text{for } a \leftarrow b. \tag{29}$$

Here, $W_\alpha^{ba} \equiv \langle b|W_\alpha|a\rangle$ with the operator W_α being defined in equation (16), $\omega_{ba}^{\mathrm{S}} = (\varepsilon_b - \varepsilon_a)/\hbar$ is the vibrational transition frequency of the reaction system, and $C_{\alpha\alpha'}(\omega)$ the substrate interaction spectrum [Eq. (21)]. The detailed-balance relation reads in the present case [44–46]

$$\gamma_1^{ba} = \mathrm{e}^{-\beta\omega_{ba}^{\mathrm{S}}} \gamma_1^{ab}. \tag{30}$$

The Bloch T_1-relaxation rate associated with $|a\rangle$ can be defined as [24,44–49]

$$\Gamma_a \equiv \sum_{b\neq a} \gamma_1^{ba}. \tag{31}$$

Next we turn to the T_2-dephasing rate between two vibrational levels, $\tilde{\gamma}_2^{ab} \equiv \mathcal{R}_{ab,ab}$. By using equation (36), we obtain [24,46–49]

$$\tilde{\gamma}_2^{ab} = \frac{1}{2}(\Gamma_a + \Gamma_b) + \gamma_2^{ab}. \tag{32}$$

Here, the first term is the T_1-induced dephasing rate, while the second term denotes the *pure* T_2-dephasing rate and can be expressed as [46]

$$\gamma_2^{ab} = \frac{1}{2}\sum_{\alpha\alpha'} C_{\alpha\alpha'}(0)(W_\alpha^{aa} - W_\alpha^{bb})(W_{\alpha'}^{aa} - W_{\alpha'}^{bb}). \tag{33}$$

Note that $\gamma_2^{ab} = \gamma_2^{ba}$. In the following, we are interested in the case where the temperature is not too low such that $C_{\alpha\alpha'}(0) \approx C_{\alpha\alpha'}^{(-)}(0)$ [*cf.* Eqs. (23–26)]. In this case, the pure dephasing stems almost exclusively from the degenerate pump-dump (Rayleigh) contribution, *i.e.*, the $j = k$ terms in equation (26) for $C_{\alpha\alpha'}^{(-)}$.

Equations (29, 33), together with formal results of the previous sections, complete the theoretical formulation of the quantum chemical construction of the Bloch-Redfield reduced equations of motion for polyatomic molecular systems such as 3CTR. In the following calculations, the summations in equations (29, 33) run over $\alpha, \alpha' = (0,1)$, (1,0), (2,0), (0,2), and (1,1); *i.e.*, we are retaining the system-substrate interaction up to the second-order in the system's Cartesian-coordinates [*cf.* Eq. (16)]. The corresponding coupling strengths of the various substrate normal modes were analyzed in Section 4.2 and are listed in Table 2. By examining equations (29, 33), and equations (23–28), we conclude that the dissipation rates are determined by the interplay between the following four factors:

(i) the overlap between the states $|a\rangle$ and $|b\rangle$ which affects the T_1-rate *via* W_α^{ab} [*cf.* Eq. (29)] and the pure T_2-rate *via* $W_\alpha^{aa} - W_\alpha^{bb}$ [*cf.* Eq. (33)];
(ii) the substrate interaction strength parameters $A_{\alpha\alpha'}(j)$ [Eq. (27)] and $B_{\alpha\alpha'}(j,k)$ [Eq. (28)], which were analyzed in Table 2 with the important substrate modes depicted in Figures 6–8;
(iii) the resonance between the system transition frequency ω_{ba}^{S} and the substrate frequency ω_j in favor of the $C^{(1)}$ contribution, or $\omega_j \pm \omega_k$ in favor of the $C^{(\pm)}$ contribution;
(iv) the density of states for a specific substrate mode j measured by the thermal occupation number $\bar{n}_j$ in equations (24–26).

Note that for pure T_2-dephasing the required interaction spectra are the $C_{\alpha\alpha'}(0) \approx C_{\alpha\alpha'}^{(-)}(0)$ contributions which are determined by $B_{\alpha\alpha'}(j,j)$ and $\bar{n}_j$ [*cf.* Eq. (26)].

Table 3. T_1-relaxation rates γ_1^{ab} [Eq. (29)] at 200 K as well as the separate contributions of the one- and two-phonon transitions. The upper/lower part corresponds to the inter-/intra-well transitions. The Bloch T_1-relaxation rates [*cf.* Eq. (31)] are $\Gamma_a = 0.0$, 0.36, 6.4, 150, 590 ps^{-1}; for $a = 0, ..., 4$, respectively. See text for details.

$a \leftarrow b$	$\omega_{ba}^{\rm S}$	γ_1^{ab}	separate contributions to γ_1^{ab}		
	(cm^{-1})	(ps^{-1})	$C^{(1)}$	$C^{(+)}$	$C^{(-)}$
$0 \leftarrow 1$	876	0.35	$1.0^{(18:1.0)}$	0.0	0.0
$0 \leftarrow 3$	2250	0.77	$0.29^{(18:0.28)}$	$0.71^{(11+18:0.32)}$	0.00
$1 \leftarrow 2$	613	0.041	$0.41^{(22:0.15)}$	$0.56^{(24+25:0.26)}$	0.03
$1 \leftarrow 4$	1510	3.3	$0.67^{(9:0.61)}$	$0.33^{(29+29:0.16)}$	0.00
$2 \leftarrow 3$	760	10	$1.0^{(18:0.92)}$	0.0	0.0
$3 \leftarrow 4$	136	12	$0.86^{(25:0.57)}$	0.05	0.09
$0 \leftarrow 2$	1489	5.4	$0.73^{(18:0.54)}$	$0.26^{(17+21:0.09)}$	0.01
$0 \leftarrow 4$	2386	6.5	$0.83^{(18:0.80)}$	$0.17^{(29+29:0.11)}$	0.00
$1 \leftarrow 3$	1374	140	$0.95^{(11:0.87)}$	0.05	0.00
$2 \leftarrow 4$	896	570	$0.99^{(18:0.99)}$	0.01	0.00

In the next subsection, these four factors will be investigated to arrive at a molecular picture for the T_1-relaxation and pure T_2-dephasing at the representative temperature of $T = 200$ K.

5.3 Molecular mechanism of dissipation

5.3.1 T_1-relaxation rates

Let us start with the molecular details of the T_1-relaxation rate γ_1^{ab} [*cf.* Eq. (29)]. Table 3 presents the calculated values of the T_1-relaxation rates γ_1^{ab} [Eq. (29)] for $a, b = 0, ..., 4$ at the temperature of 200 K. The corresponding transition frequencies $\omega_{ba}^{\rm S}$ in the reactive system are also given. The γ_1^{ab} (with $a > b$) which are not shown explicitly can be evaluated *via* the detailed-balance relation [Eq. (30)]. We also give the Bloch T_1-relaxation rates Γ_a [Eq. (31)] associated with the individual levels. The left three columns of Table 3 list the separate contributions to γ_1^{ab} assuming that the substrate interaction spectrum $C_{\alpha\alpha'}$ in equation (29) is divided into its three components, $C_{\alpha\alpha'}^{(1)}, C_{\alpha\alpha'}^{(+)}$, and $C_{\alpha\alpha'}^{(-)}$, respectively [*cf.* Eq. (23)]. In order to elucidate which modes contribute most to theses coefficients we give the mode index as well as the respective relative contribution as superscripts. Consider, for example, the $0 \leftarrow 2$ transition which has a total rate of $\gamma_1^{02} = 5.4$ ps^{-1}. The contribution of ω_{18} is 54% (*via* $C^{(1)}$) and that of ω_{17} and ω_{21} is 9% (*via* $C^{(+)}$). Note that the small contribution of $C^{(-)}$ to the T_1-rates shown in Table 3 is not a general rule. In fact, the $C^{(-)}$'s contribution to γ_1^{35} which is not listed is 76%. The upper and lower parts of Table 3 are for the *inter-well* and *intra-well* transitions, respectively (*cf.* Fig. 5). The overall T_1-rates γ_1^{ab} for the inter-well transitions are smaller than those for the intra-well transitions. As will be shown later this behavior is just opposite to that of the pure T_2-dephasing.

Table 4. Pure T_2-dephasing rates γ_2^{ab} [Eq. (33)] at 200 K. The upper/lower part corresponds to the inter-/intra-well transitions. Given are also the separate contributions from the indicated substrate modes *via* the degenerate pump-dump ($C^{(-)}$) coupling.

$a \leftarrow b$	γ_2^{ab}	jth mode contribution			
	(ps^{-1})	$j = 25$	29	36	37
$0 \leftarrow 1$	3200	0.61	0.08	0.23	0.01
$0 \leftarrow 3$	2200	0.57	0.12	0.18	0.05
$1 \leftarrow 2$	3200	0.62	0.08	0.21	0.01
$1 \leftarrow 4$	3900	0.51	0.04	0.24	0.14
$2 \leftarrow 3$	2100	0.60	0.11	0.17	0.04
$3 \leftarrow 4$	2300	0.57	0.07	0.24	0.04
$0 \leftarrow 2$	5.0	0.02	0.10	0.21	0.58
$0 \leftarrow 4$	410	0.00	0.03	0.03	0.93
$1 \leftarrow 3$	350	0.23	0.00	0.13	0.62
$2 \leftarrow 4$	350	0.00	0.02	0.06	0.91

The above details of the state-to-state T_1-rates can be explained as resulting from the interplay between the four factors listed at the end of the last subsection. Factor (i), *i.e.* the overlap between $|a\rangle$ and $|b\rangle$ accounts for the overall large T_1-rates for the intra-well transition (lower part of Tab. 3) in comparison with those for the inter-well transition (upper part of Tab. 3). Factor (ii), *i.e.* the substrate interaction strength accounts for the overall importance of substrate modes with $j = 18$, 25 and 29 (*cf.* Tab. 2) in many of the $C^{(1)}$'s and $C^{(+)}$'s contributions to γ_1^{ab}. The molecular pictures of these strong coupling substrate modes were described in Section 4.2 and Figures 6 and 7a. Factor (iii), *i.e.* resonance accounts for other specific substrate modes, such as $\omega_{24} + \omega_{25} = 612$ cm^{-1} matching well with $\omega_{21}^{\rm S} = 613$ cm^{-1} (for $1 \leftarrow 2$), contributing significantly to specific state-to-state T_1-relaxations (*cf.* Tab. 3). Factor (iv), *i.e.* $\bar{n}_j$ affects the values of γ_1^{ab} but introduces no substrate mode-selectivity in the present case of the T_1-relaxation rates. However, it will be shown to be an important factor for the substrate mode-selectivity in γ_2^{ab}.

5.3.2 Pure T_2-dephasing rates

We now turn to the molecular origin of the pure T_2-dephasing rates γ_2^{ab}. Table 4 presents the calculated γ_2^{ab}; with $a, b = 0, ..., 4$ at the temperature of 200 K, together with the individual contributions from the four important substrate modes $j = 25, 29, 36$, and 37. The table is also partitioned into inter-well (upper part) and intra-well (lower part) transitions. The presented pure-T_2 rates can be analyzed in terms of three related aspects:

(a) the molecular patterns of important substrate normal modes;
(b) the physical picture of pure-dephasing between two states originating from the fluctuation of the associated transition frequency;

(c) the interplay among the factors (i–iv) described earlier in Section 5.2.

First, we observe that the overall pure-dephasing rates for the inter-well transitions (upper part of Tab. 4) are much larger than their intra-well counterparts (lower part of Tab. 4). This behavior can be understood in terms of the $\propto (W_\alpha^{aa} - W_\alpha^{bb})$ dependence of the dephasing rates which gives a larger contribution for inter-well transition frequency fluctuations. This behavior is just opposite to the T_1-relaxation case due to factor (i) (overlap between wave functions) which favors W_α^{ab} in equation (29) for the T_1-rates, but discriminates against $W_\alpha^{aa} - W_\alpha^{bb}$ in equation (33) for the T_2-rates. As a result, the inter-well γ_2 (γ_1) rates are larger (smaller) than the intra-well counterparts (comp. Tabs. 4 and 3). Detailed analysis shows that pure T_2-dephasing is almost exclusively coming from the coupling of the system's x-coordinate; *i.e.*, of W_α with $\alpha = (1,0)$ and $(2,0)$.

We now turn to the four important substrate modes $j = 25, 29, 36$, and 37 that contribute in total over 90% to the γ_2^{ab} for each $a \leftrightarrow b$ pair. As mentioned earlier, pure dephasing stems almost exclusively from the Rayleigh pump-dump contribution due to each individual substrate normal mode; *i.e.*, from the $j = k$ terms in equation (26) for $C_{\alpha\alpha'}^{(-)}(0) \approx C_{\alpha\alpha'}(0)$ which contributes to γ_2^{ab} [Eq. (33)]. Both the values of $B_{\alpha\alpha}(j,j)$ [factor (ii)] and the thermal occupation number $\bar{n}_j$ [factor (iv)] play a role [*cf.* Eq. (26)]. In fact, as far as the values of $B_{\alpha\alpha}(j,j)(\bar{n}_j+1)\bar{n}_j$ are concerned (*cf.* Tab. 2), mode 37 > mode 29 > mode 36 > mode 25. Other modes, including $j = 18$ and 30 [*cf.* Figs. 6a and 7b] which have significant values of $B_{\alpha\alpha}(j,j)$, are at least one order of magnitude smaller in terms of $B_{\alpha\alpha}(j,j)(\bar{n}_j+1)\bar{n}_j$ at the considered temperature.

The fact that mode $j = 37$ gives the dominant contribution to the intra-well pure dephasing may be understood using the above reasoning. However, the observation that the dominant *inter-well pure dephasing substrate modes* are $j = 25$ and 36, rather than $j = 29$ and 37, which have $B_{\alpha\alpha}(j,j)(\bar{n}_j+1)\bar{n}_j$ values larger than those of the former two modes, is surprising. Mathematically, it results from the fact that the former/latter two modes are subject to enhancement/cancellation as the summations in equation (33) are carried out.

To understand this seemingly peculiar observation on the selective enhancement/cancellation, let us examine the molecular motions in of modes $j = 25$ and 36 *versus* those of modes $j = 29$ and 37, in order to establish a physical picture of pure dephasing. The substrate normal mode $j = 25$ [Fig. 6b] involves an in-plane quasi-rotation of all atoms, except for the counter-clockwise motion of the Cl. The substrate normal mode $j = 36$ [Fig. 8a] involves an out-of-plane motion of the substrate atoms and the z-direction motion of the proton parallel to one O atom and anti-parallel to the other O atom. Both modes 25 and 36 have a large bias in relation to the two wells, leading to enhanced contributions to inter-well pure dephasing. The mode $j = 37$ [Fig. 8b] is much like the mode $j = 36$, but does not involve large motion of the proton in z-direction. As a result, the mode $j = 37$ has no bias against different wells, which implies a cancellation as the summations in equation (33) is carried out for the inter-well pure dephasing rates. The mode $j = 29$ [Fig. 7a] involves essentially the motion of the proton in z-direction with also no bias against the two O atoms, and hence the two wells. Therefore, the modes 37 and 29 do not contribute as much as the modes 25 and 36 to the *inter-well* pure dephasing, in spite of the mode 37 being the dominant contribution to the *intra-well* pure dephasing.

6 Summary

We have presented the complete procedure for the quantum chemical construction of the Hamiltonian and the relaxation rates for proton transfer reactions in large molecules, exemplified *via* an isolated 3-chlorotropolone molecule at finite temperature. This was done by combining the all-Cartesian system-plus-substrate Hamiltonian construction (Sect. 2) with a quantum dissipation formulation (Appendix A). For the intramolecular PT in 3CTR, we treated the (x,y)-coordinates of the reactive H atom as the reduced system, and the remaining 37 internal substrate modes as the intramolecular bath which was assumed to be Markovian. The reduced reaction system Hamiltonian (Sect. 3), the bath interaction spectra (Sect. 4), and the state-to-state T_1-relaxation and pure T_2-dephasing rate constants (Sect. 5) can thus been identified at a high level of quantum chemistry.

It should be emphasized that treating the intramolecular PT in an isolated molecule in terms of dissipation dynamics is an approximation due to the finite number of substrate degrees of freedom. However, the resulting information, such as the temperature-dependent effective reaction Hamiltonian and T_1- and T_2-rates, support the semi-quantitative nature of our study of the primary dynamical event of interest in the considered molecule. More importantly, the present method allows to identify important collective motions (*i.e.*, the substrate normal modes) individually in terms of their coupling strengths and their specific effects on the population or/and phase dynamics in the reduced reaction system. In particular, we have demonstrated (*cf.* Sect. 5.3.2) the importance of biquadratic system-substrate couplings in determining the state-to-state phase dynamics (in terms of pure T_2-dephasing). To our knowledge, such a molecular level analysis of pure dephasing has never been carried out before for a PT system.

The electronic spectroscopies applied to tropolone derivatives so far have been focused on certain optical active collective modes, where the information of PT is deduced indirectly *via* its effects such as frequency-shift and line-splitting on the normal modes [28–34]. A possible approach to the direct measurement of ground state PT is Raman or multi-dimensional vibrational spectroscopy [50]. On the other hand, ultrafast mid-IR four-wave mixing studies on non-reactive hydrogen-bonded complexes have been reported recently [36,37]. In this respect it is interesting to note that for the hydrogen

bonded network in HOD/D_2O [36] as well as for the intramolecular medium strong hydrogen bond in phthalic acid monomethylester in CCl_4 [37], photon echo data revealed pure dephasing times below 100 fs. In the latter case it was concluded that intramolecular (anharmonic coupling) as well as solvent (homogeneous broadening) effects could be responsible for this short dephasing time. The present calculation suggests that a system with an intramolecular hydrogen-bond can in principle exhibit ultrafast pure dephasing even in the gas phase.

A novel feature of this work is the establishment of the correlation between the pattern of substrate mode vibrations and the inter-well/intra-well pure dephasing processes they induce. This correlation together with its T_1-relaxation counterpart was discussed in detail in Section 5 and highlighted in Tables 3, 4, and Figures 6–8. The modes 25 and 37 [Figs. 6b and 8b] are identified as the substrate motions most responsible for the inter-well and intra-well pure dephasing processes, respectively, in the PT in 3CTR at $T = 200$ K (*cf.* Tab. 4). The mode 25 (37) is also the lowest frequency in-plane (out-of-plane) substrate mode, whereas the PT corresponds to the reactive H atom's in-plane motion. The seemingly peculiar substrate mode-selectivity in the inter-well/intra-well pure dephasing described above was elucidated in detail in Section 5.3.2 *via* the patterns of substrate motion, in relation to the physical picture and the formulation [Eq. (33)] of pure dephasing.

In terms of the overall coupling strength (*cf.* Tab. 2), the most important substrate motion is due to mode 18 [Fig. 6a]. This mode has promoting character for the PT. It's exceptional role is in accord with the general picture of PT reactions [9,51,52]. It should be emphasized that our partitioning of the total Hamiltonian into a system and a bath part was to some extent guided by the separation into anharmonic and harmonic motions. Keeping the system part two-dimensional facilitated a straightforward analysis of the resulting relaxation rates with their microscopic explanation being more important than their absolute values. The promoting mode $j = 18$ would, of course, be the primary candidate for inclusion into the system part. The strong coupling to mode 18 also raises the question whether this mode can be treated in the harmonic limit, in particular in the E2 potential well. One way of dealing with this problem would be to stay with the harmonic approximation but to use a flexible substrate reference geometry [7] which would reduce the overall force on the substrate atoms. Alternatively, mode 18, for example, could be considered explicitly in the quantum chemistry calculation as well which would account for the full anharmonicity of this degree of freedom.

This work has been financially supported by the Research Grants Council of the Hong Kong Government, the National Natural Science Foundation of China, the Deutsche Forschungsgemeinschaft through the Sfb 450, and the DAAD. We are grateful to Professor J. Manz for useful discussions and critical comments. Finally, R. Xu would like to express her heartfelt appreciation to Prof. J. Manz and Mrs. A. Polinske for their hospitality during her four-month visit to FU Berlin.

Appendix A: Bloch–Redfield theory

The Redfield equation of motion can be expressed in the following algebraic form [44,46]:

$$\dot{\rho} = -\mathrm{i}[H,\rho] - \frac{1}{2}\sum_{\alpha}[W_\alpha, \tilde{W}_\alpha\rho - \rho\tilde{W}_\alpha^\dagger], \tag{34}$$

$$\tilde{W}_\alpha \equiv \sum_{\alpha'} C_{\alpha\alpha'}(-\mathcal{L})W_{\alpha'}. \tag{35}$$

Here, H is the effective reaction Hamiltonian whose PES in the Cartesian coordinates is given by equation (10), W_α is defined in equation (16), while $C_{\alpha\alpha'}(-\mathcal{L})$ is a function of the reduced system Liouvillian operator $\mathcal{L} \equiv [H, \bullet]$, defined by the bath interaction spectrum $C_{\alpha\alpha'}(\omega)$ [Eq. (21)]. As the spectrum is real [*cf.* Eqs. (23–28)], we have $\tilde{W}_\alpha^\dagger = \sum_{\alpha'} C_{\alpha\alpha'}(\mathcal{L})W_{\alpha'}$. By using the spectral detailed-balance relation, equation (22), one can easily show that $\rho_{\mathrm{eq}} \propto \exp(-\beta H)$ is a stationary solution to the Redfield equation (34).

The second term in equation (34) can be recast in the form, $-\mathcal{R}\rho$, where $\mathcal{R}$ is the dissipation superoperator or tensor. The Redfield dissipation tensor elements in the H-eigenstate $\{|a\rangle\}$-representation can be obtained as [46]

$$\mathcal{R}_{ab,a'b'} = (\mathcal{K}_{ab,a'b'} + \mathcal{K}^*_{ba,b'a'})/2, \tag{36}$$

$$\mathcal{K}_{ab,a'b'} = \sum_{\alpha}[\delta_{bb'}(W_\alpha\tilde{W}_\alpha)_{aa'} - W_\alpha^{b'b}\tilde{W}_\alpha^{aa'}]. \tag{37}$$

The Redfield equation, equation (34), does not preserve the positivity [45,46] and may lead to non-physical results of $\rho_{aa} < 0$, especially when the system–bath coupling is strong.

Alternatively, one may consider the so-called secular approximation which retains only the diagonal dissipation tensor elements, $\mathcal{R}_{aa,bb}$ and $\mathcal{R}_{ab,ab}$. This approximation amounts to the following Bloch equations (in the diagonal H-representation):

$$\dot{\rho}_{aa} = -\mathrm{i}[H,\rho]_{aa} - \Gamma_a\rho_{aa} + \sum_{b\neq a}\gamma_1^{ab}\rho_{bb}, \tag{38}$$

$$\dot{\rho}_{ab} = -\mathrm{i}[H,\rho]_{ab} - \tilde{\gamma}_2^{ab}\rho_{ab}. \tag{39}$$

Here, $\gamma_1^{ab} \equiv -\mathcal{R}_{aa,bb}$ and $\tilde{\gamma}_2^{ab} \equiv \mathcal{R}_{ab,ab}$, which can be evaluated *via* equation (36). The rates are given explicitly in equations (29, 32) with (33), whereas Γ_a is defined in equation (31).

References

1. E. Kraka, in *Encyclopedia Computational Chemistry*, edited by P. von Rague-Schleyer (Wiley, New York, 1998), p. 2437.

2. *The Reaction Path in Chemistry: Current Approaches and Perspectives*, edited by D. Heidrich (Kluwer Academic, Dordrecht, 1995).
3. W.H. Miller, N.C. Handy, J.E. Adams, J. Chem. Phys. **72**, 99 (1980).
4. J.T. Carrington, W.H. Miller, J. Chem. Phys. **84**, 4364 (1986).
5. N. Shida, P.F. Barbara, J.E. Almlöf, J. Chem. Phys. **91**, 4061 (1989).
6. E.B. Wilson, J.C. Decius, P.C. Cross, *Molecular Vibrations: The Theory of Infrared and Raman Vibrational Spectra* (McGraw-Hill Book Company, Inc., N.Y., 1955).
7. B.A. Ruf, W.H. Miller, J. Chem. Soc., Faraday Trans. 2 **84**, 1523 (1988).
8. A.E. Orel, O. Kühn, Chem. Phys. Lett. **304**, 285 (1999).
9. H. Naundorf, J.A. Organero, A. Douhal, O. Kühn, J. Chem. Phys. **110**, 11286 (1999).
10. A.E. Orel, Y. Zhao, O. Kühn, J. Chem. Phys. **112**, 94 (2000).
11. K. Yagi, T. Taketsugu, K. Hirao, J. Chem. Phys. **115**, 10647 (2001).
12. R.B. Gerber, V. Buch, M.A. Ratner, J. Chem. Phys. **77**, 3022 (1982).
13. R.B. Gerber, M.A. Ratner, V. Buch, Chem. Phys. Lett. **91**, 173 (1982).
14. H.D. Meyer, U. Manthe, L.S. Cederbaum, Chem. Phys. Lett. **165**, 73 (1990).
15. U. Manthe, H.D. Meyer, L.S. Cederbaum, J. Chem. Phys. **97**, 3199 (1992).
16. M.H. Beck, A. Jäckle, G.A. Worth, H.D. Meyer, Phys. Rep. **324** (2000).
17. A.B. McCoy, R.B. Gerber, J. Chem. Phys. **101**, 1975 (1994).
18. A. Roitberg, R.B. Gerber, R. Elber, M.A. Ratner, Science **268**, 1319 (1995).
19. G.K. Paramonov, H. Naundorf, O. Kühn, Eur. Phys. J. D **14**, 205 (2001).
20. H. Naundorf, G.A. Worth, H.-D. Meyer, O. Kühn, J. Phys. Chem. A **106**, 719 (2002).
21. K. Blum, *Density Matrix Theory and Applications* (Plenum, New York, 1981).
22. A.J. Leggett, S. Chakravarty, A.T. Dorsey, M. Gary, Rev. Mod. Phys. **59**, 1 (1987).
23. U. Weiss, *Quantum Dissipative Systems*, 2nd edn. (World Scientific, Singapore, 1999), Series in Modern Condensed Matter Physics, Vol. 10.
24. V. May, O. Kühn, *Charge and Energy Transfer Dynamics in Molecular Systems* (Wiley-VCH, Berlin, 2000).
25. N. Došlić, K. Sundermann, L. González, O. Mó, J. Giraud-Girard, O. Kühn, Phys. Chem. Chem. Phys. **1**, 1249 (1999).
26. O. Kühn, Eur. Phys. J. D **6**, 49 (1999).
27. N. Došlić, O. Kühn, Chem. Phys. **255**, 247 (2000).
28. H. Sekiya, Y. Nagashima, Y. Nishimura, J. Chem. Phys. **92**, 5761 (1990).
29. T. Tsuji, H. Sekiya, S. Ito, H. Ujita, M. Habu, A. Mori, H. Takeshita, Y. Nishimura, J. Chem. Phys. **98**, 6571 (1993).
30. F.A. Ensminger, J. Plassard, T.S. Zwier, S. Hardinger, J. Chem. Phys. **99**, 8341 (1993).
31. H. Sekiya, T. Tsuji, S. Ito, A. Mori, H. Takeshita, Y. Nishimura, J. Chem. Phys. **101**, 3464 (1994).
32. H. Hamabe, T. Fukuchi, S. Shiraishi, K. Nishi, Y. Nishimura, T. Tsuji, N. Nishi, H. Sekiya, J. Phys. Chem. A **102**, 3880 (1998).
33. K. Nishi, H. Sekiya, H. Kawakami, A. Mori, Y. Nishimura, J. Chem. Phys. **109**, 1589 (1998).
34. K. Nishi, H. Sekiya, H. Kawakami, A. Mori, Y. Nishimura, J. Chem. Phys. **111**, 3961 (1999).
35. J. Stenger, D. Madsen, J. Dreyer, E.T.J. Nibbering, P. Hamm, T. Elsaesser, J. Phys. Chem. A **105**, 2929 (2001).
36. J. Stenger, D. Madsen, P. Hamm, E.T.J. Nibbering, T. Elsaesser, Phys. Rev. Lett. **87**, 027401 (2001).
37. J. Stenger, D. Madsen, J. Dreyer, P. Hamm, E.T.J. Nibbering, T. Elsaesser, Chem. Phys. Lett. **354**, 256 (2002).
38. M.J. Frisch *et al.*, *Gaussian 98, Revision A.6*, Pittsburgh PA, Gaussian 98 Inc., 1998.
39. A.O. Caldeira, A.J. Leggett, Physica A **121**, 587 (1983).
40. A.O. Caldeira, A.J. Leggett, Ann. Phys. (N.Y.) **149**, 374 (1983).
41. R.X. Xu, Y.J. Yan, unpublished.
42. J.C. Light, I.P. Hamilton, J.V. Lill, J. Chem. Phys. **82**, 1400 (1985).
43. C.C. Marston, G.G. Balint-Kurti, J. Chem. Phys. **91**, 3571 (1989).
44. A.G. Redfield, Adv. Magn. Reson. **1**, 1 (1965).
45. W.T. Pollard, A.K. Felts, R.A. Friesner, Adv. Chem. Phys. **93**, 77 (1996).
46. Y.J. Yan, F. Shuang, R.X. Xu, J.X. Cheng, X.Q. Li, C. Yang, H.Y. Zhang, J. Chem. Phys. **113**, 2068 (2000).
47. R.K. Wangsness, F. Bloch, Phys. Rev. **89**, 728 (1953).
48. F. Bloch, Phys. Rev. **105**, 1206 (1957).
49. O. Kühn, Y. Zhao, F. Shuang, Y.J. Yan, J. Chem. Phys. **112**, 6104 (2000).
50. S. Mukamel, Ann. Rev. Phys. Chem. **51**, 691 (2000).
51. S. Scheiner, in *Proton Transfer in Hydrogen–bonded Systems*, edited by T. Bountis (Plenum Press, New York, 1992), p. 17.
52. V.A. Benderskii, E.V. Vetoshkin, I.S. Irgibaeva, H.P. Trommsdorff, Chem. Phys. **262**, 393 (2000).